Experimental Study of the Aerodynamics of Incipient Torsional Stall Flutter

F. O. Carta* and P. F. Lorber†
United Technologies Research Center, East Hartford, Connecticut

An experimental study has been made of the aerodynamics of small-amplitude airfoil torsional oscillations near stall to examine the mechanism that leads to stall flutter on propeller blades. An airfoil was oscillated in pitch at amplitudes of 0.5, 2.0, and 4.0 deg. Time histories of the unsteady surface pressures show that stall initiation and reattachment at low amplitudes are determined not only by kinematic conditions but also by the presence or absence of random effects such as gusts or vibrations. In contrast to the results at higher amplitude, hysteresis loops at low amplitude near stall are dominated by a central destabilizing subloop, so that the aerodynamic pitch damping per unit amplitude has a maximum negative value near an amplitude of 2 deg. This implies that small-amplitude oscillations near stall may be extremely unstable. The measured aerodynamic damping is used in a model calculation to predict the growth rate of torsional oscillations of an airfoil free to oscillate in pitch. An initial small torsional disturbance grows rapidly and then asymptotically approaches a limiting amplitude, a behavior similar to that observed during stall flutter.

Nomenclature

$\mathcal{R}$ = aspect ratio, L/c
c = airfoil chord
C_M = pitching moment coefficient about $x/c=0.25$, M/qc^2
C_N = normal force coefficient
C_P = pressure coefficient $(P-P_\infty)/q$
$C_{\bar{\xi}}$ = damping constant, Eq. (7)
G = modulus of torsional rigidity, psi
I = mass moment of inertia about $x/c=0.25$
k = reduced frequency, $\omega c/2U_\infty$
K = torsional spring constant
L = model blade span
M = aerodynamic moment
M_∞ = Mach number
P_∞ = freestream static pressure
q = freestream dynamic pressure, $\rho U_\infty{}^2/2$
x = distance along chord from leading edge
U_∞ = freestream velocity
α = geometric angle of attack, $\alpha=\alpha_0+\tilde{\alpha}\sin\omega t$, deg
α_0 = time mean angle of attack
$\tilde{\alpha}$ = amplitude of oscillation
α_{ss} = static stall angle
ρ = air density
ρ_m = material density of blade
τ = airfoil thickness to chord ratio
ϕ = angle of phase lead
ω = frequency, $2\pi f$, rad/s

Introduction

FOR a period of time during the 1950s, the propeller stall flutter problem was actively studied as designers realized that the thinner blade sections required for high speed performance were susceptible to self-induced torsional flutter. This stall-related instability was encountered primarily at static thrust or low-speed-takeoff conditions, with blades operating at high angles of attack. Its characteristic behavior was a small-amplitude initiation at or near the static stall angle, a rapid growth to a large amplitude, and a reduction in growth rate to a final constant amplitude, termed a limit-cycle oscillation.

Typical of the approach used at that time, Ref. 1 explored the effects of several parameters on stall flutter but was restricted to a phenomenological description of flutter in terms of a stability boundary. This boundary separated the safe operating regime from a hazardous zone which, if penetrated too deeply, could lead to overstressing the propeller blade. Such a phenomenological approach represented a first step toward providing a rational design procedure and was followed by attempts to better define the flutter boundary of representative airfoil sections[2] and to quantify the approach to the boundary by measuring aerodynamic damping.[3] All these approaches were based on gross section measurements employing relatively insensitive strain gage instrumentation to record damping decay (or growth) of the airfoil elastic response. The data so obtained were inadequate for accurate design estimates and useless for obtaining an understanding of the underlying mechanism. Before improvements could be made in measurement devices and techniques, the widespread use of gas turbines for aircraft directed most of the research away from propeller flutter and toward compressor blade instabilities. Concurrently, a demand for better performance in helicopters led to an active research program on the dynamic stall process during large-amplitude pitching motions.

A large and well-documented body of literature exists on the measurement and interpretation of unsteady aerodynamics relevant to helicopter rotor blades operating in the dynamic stall regime.[4-9] The results of these studies are specifically suited to helicopter blade parameter ranges and behavior, involving simulations of large cyclic pitch changes about a quarter-chord pivot axis, with significant stall penetration of a typical helicopter airfoil section at Mach numbers generally less than 0.5. This has provided the helicopter industry with the data needed to predict the large unsteady loads associated with dynamic stall on the retreating side of the rotor disk.

In striking contrast to the large-amplitude pitching excursions of the helicopter rotor blade, the dynamic stall problem of the propeller blade begins with an incipient torsional motion in the vicinity of the static stall point. Although it has

Received March 21, 1986; presented as Paper 86-0901 at the AIAA/ASME/ASCE/AHS 27th Structures, Structural Dynamics and Materials Conference, San Antonio, TX, May 19-21, 1986; revision received July 26, 1986.

*Supervisor, Aerodynamics. Associate Fellow AIAA.
†Associate Research Engineer. Member AIAA.

long been conjectured that the growth of the self-induced stall flutter motion is linked to a variation in aerodynamic damping with pitching amplitude, no measurements have been published prior to the current study to substantiate this presumption. This is due partly to the relative insensitivity of most measurement devices (such as miniature pressure transducers) and the consequent difficulty in separating the coherent periodic signal from the background noise at small amplitudes. The recent demonstration of our ability to make such measurements successfully in a cascade experiment[10] led directly to this first pilot experiment to measure blade loadings under simulated incipient motion conditions. The results obtained are encouraging and, although preliminary, they appear to corroborate the conjecture cited above and lead directly to a prediction of a realistic self-induced limit-cycle oscillatory behavior.

Experiment

The experiment was performed in the UTRC oscillating cascade wind tunnel,[10] as modified to perform isolated airfoil tests.[5] An existing airfoil model was used. It had a 9.5%-thick Sikorsky SC1095 profile (Fig. 1) with a 15.24-cm (6-in.) chord and a 25.4-cm (10-in.) span. The airfoil was driven in a sinusoidal pitching motion through a four-bar linkage. Three different cams were used to produce pitching amplitudes of 0.5, 2.0, and 4.0 deg. Complete details of the model and its installation are given in Ref. 5.

Ten miniature pressure transducers were mounted in a Gaussian array on each airfoil surface along the center span, as shown in Fig. 1. Each transducer output was ac-coupled to yield only the oscillatory component, with the time-mean pressures being determined by pneumatic orifices located next to each transducer. The estimated accuracy of the time-mean pressures is 0.5% of the full-scale range, while the accuracy of the unsteady pressures is approximately 2%. Unsteady pressures were digitized on-line, with between one and ten ensembles of 1024 samples per transducer recorded at each test point. Following the test, the unsteady and time-mean pressures were combined, converted to pressure coefficient, ensemble-averaged, and Fourier-analyzed. Per-unit-span normal force and pitching moment coefficients (about the quarter-chord) were computed, assuming the flow to be two-dimensional near midspan.

All data reported here were taken at a wind tunnel freestream velocity of 61 m/s (200 ft/s). This corresponds to a Reynolds number based on airfoil chord of 650,000, and a Mach number of 0.18. Steady pressure distributions were obtained over an angle of attack range of 0–18 deg. Unsteady data were obtained at 54 combinations of mean angle, oscillation amplitude, and frequency in the range:

$$8.0 < \alpha_0 < 10.5 \text{ deg}$$

$$0.5 < \bar{\alpha} < 4.0 \text{ deg}$$

$$4.0 < f < 20 \text{ Hz}$$

Pressure, Force, and Moment Results

The steady flow stall angle of this airfoil is approximately 9.5 deg, as shown by the normal force and pitching moment curves in Fig. 2. The steady results are given by the solid curves and open symbols. The data were taken in a single continuous run by increasing the angle of attack from 10 to 12.5 deg (unflagged symbols), decreasing from 12.5 to 8 deg (singly flagged symbols), and finally increasing again back to 10 deg (doubly flagged symbols). All the points appear to fall on the same curve to within experimental accuracy, which indicates that there is no hysteresis for this particular steady flow. The stall is quite sudden and repeatable, although the actual drops in force and moment at stall are not large ($\Delta C_N = 0.12$, $\Delta C_M = 0.07$). The nearly constant post-stall pressure distributions on the suction surface (not shown) indicate that the flow separates over nearly the entire surface. This type of behavior normally corresponds to a leading-edge stall.

Over the tested range of reduced frequencies ($0.05 < k < 0.16$) there are no observed qualitative changes in the character of the flow. There are, however, quantitative differences reflected in the mean force and moment results. The closed symbols in Fig. 2 represent the time-mean values taken at an oscillation amplitude of 2 deg. In fully attached flow at $\alpha_0 = 8$ deg, there are no significant differences with reduced frequency. At mean angles near stall, the mean force and moment represent combinations of stalled and unstalled values. At higher reduced frequency, the airfoil is stalled over a smaller fraction of the period than at low reduced frequency. The larger unstalled loads therefore contribute a greater share of the overall loading at higher frequency, resulting in an increase in the time-mean force and moments with reduced frequency. Note also that the combination of stalled and unstalled flow tends to replace the sharp changes in the steady normal force and moment curves with smooth transitions through the stall region.

The time-dependent normal force and moment were Fourier-analyzed to generate amplitudes and phases at the fundamental frequency and its harmonics. The amplitude of the normal force coefficient at the fundamental is normalized by dividing by the angular amplitude of the oscillation (in radians). For a quasisteady attached flow with a linear lift curve, the value of $\overline{C_N}/\bar{\alpha}$ would be the lift curve slope which, for this experiment, was measured in steady flow as 4.07/rad. Figure 3 shows the variation of $\overline{C_N}/\bar{\alpha}$ with mean angle at four reduced frequencies and at oscillation

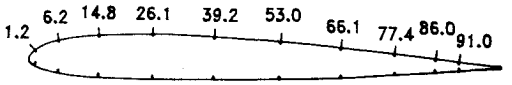

Fig. 1 SC1095 airfoil with pressure transducer locations (% x/c).

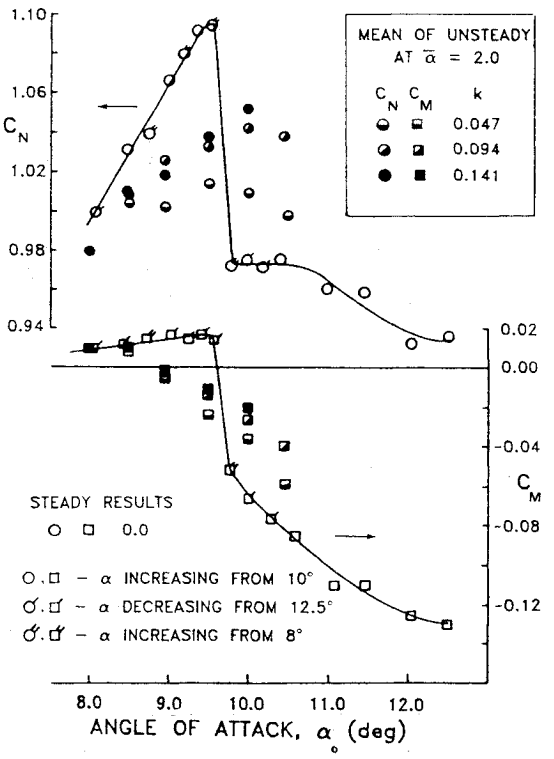

Fig. 2 Mean normal force and pitching moment.

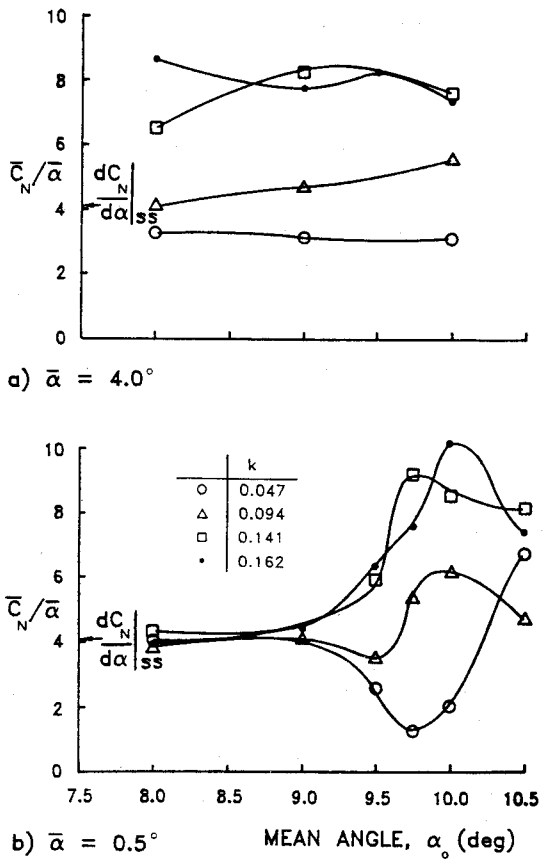

Fig. 3 Normal force amplitude at fundamental frequency.

amplitudes of 0.5 and 4 deg. At $\bar{\alpha}=4$ deg (Fig. 3a), $\overline{C_N}/\bar{\alpha}$ is larger at higher values of k but shows no clear trend with α_0. At $\bar{\alpha}=0.5$ deg (Fig. 3b), $\overline{C_N}/\bar{\alpha}$ depends much more strongly on α_0. When the maximum instantaneous angle ($\alpha_0+\bar{\alpha}$) is less than the static stall angle (α_{ss}), $\overline{C_N}/\bar{\alpha}$ is nearly independent of α_0 and is equal to the lift curve slope. At larger angles $\overline{C_N}/\bar{\alpha}$ shows a strong dependence on α_0. At the lowest reduced frequency ($k=0.047$) $\overline{C_N}/\bar{\alpha}$ drops by 60% at the stall angle (9.75 deg) and then increases rapidly. This behavior is similar to that expected for a quasisteady small disturbance, since the amplitude of such a disturbance would be proportional to the absolute value of the steady lift curve slope. Examination of Fig. 2 indicates that $d(\overline{C_N})/d(\bar{\alpha})$ is approximately constant below stall, has a minimum at the maximum lift angle (9.5 deg), and attains a large negative value during stall (between 9.5 and 9.8 deg). In the low-frequency, unsteady results (Fig. 3), there appears to be a small (0.25-deg) delay in the angle of minimum $\overline{C_N}/\bar{\alpha}$ and some smoothing of the curve, demonstrating that even the case of $k=0.047$, $\bar{\alpha}=0.5$ is not a pure quasisteady small disturbance. At higher reduced frequencies, the $\overline{C_N}/\bar{\alpha}$ curve departs further from the quasisteady behavior, missing the minimum that corresponds to the angle of $C_{N,\max}$, and having maxima that occur at 9.75 deg for $k=0.141$ and at 10.25 deg for $k=0.162$.

Time Histories

Considerable qualitative information regarding the nature of the unsteady flowfield may be obtained by examining the instantaneous time histories of the pressure measurements. This includes the flow state (stalled or unstalled), the harmonic content, and the level of variations of both small time scale (turbulence) and large time scale (cycle-to-cycle repeatability). Separation may be identified by an abrupt change (in time) in level of the pressure and by an increase in the intensity of the random fluctuations.

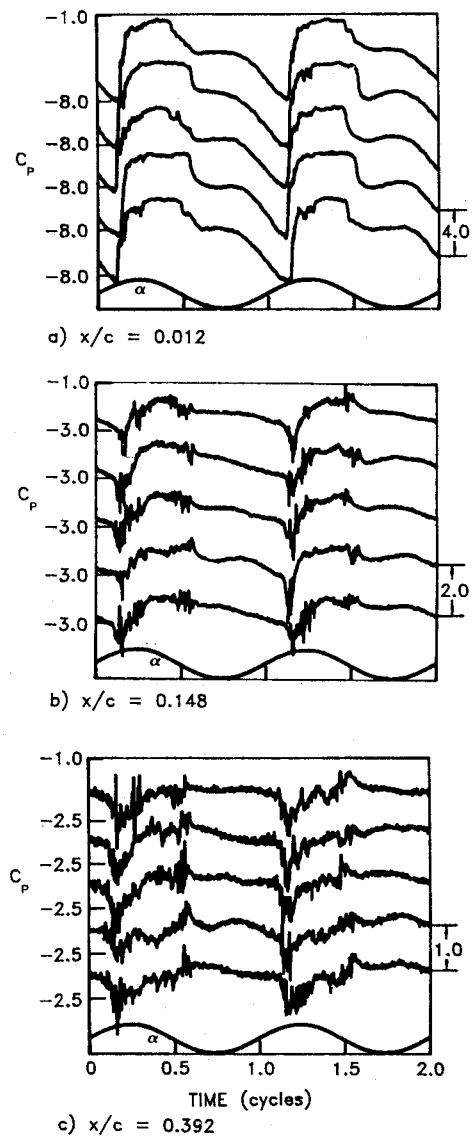

Fig. 4 Time histories of the suction surface pressure coefficient ($\alpha=10$ deg + 4 deg sinωt, $k=0.094$).

These features are most clearly defined when the airfoil oscillates near stall at a moderate amplitude and frequency. Time histories of the pressures on the suction surface at three chordwise locations are shown in Fig. 4 for the case of $\alpha=10+4\cos\omega t$ at $k=0.094$. Five nonconsecutive sequences of data are presented in each panel. The time origin of each sequence coincides with $\alpha=\alpha_0$, and each sequence covers two oscillation cycles. The bottom curve in each panel represents the angle of attack. For clarity the sequences are offset vertically as indicated on the right side of each panel.

The sequences vary in detail, but exhibit similar overall characteristics. The most dramatic variations occur near the suction peak, as shown in Fig. 4a, at $x/c=0.012$. Near $t=0$, the flow is attached, and C_P becomes more negative as t and α increase. C_P reaches a minimum value of approximately -8 prior to separation. Separation is very abrupt and does not occur at exactly the same angle in each time sequence. Following separation, C_P remains relatively constant at values between -1 and -2 until reattachment, which also occurs at a slightly different angle in each sequence.

Further downstream on the suction surface at $x/c=0.148$ (Fig. 4b), the changes in the level of C_P are reduced from those observed near the suction peak, but regions of separated and unseparated flow are still well differentiated by the increased small-scale variations in the separated

regions. There is also a sharp negative peak in C_P that may correspond to the passage of the separation vortex. At $x/c=0.392$ (Fig. 4c), this peak weakens, and the differences in the magnitudes of the small-scale variations are reduced.

At other reduced frequencies and mean angles of attack (not shown), the primary observed changes in the time sequences involve the size and location (in time) of the separated flow region. In general, and as would be expected, increasing α_0 increases the fraction of the time that the flow is separated, while increasing k delays the onset of stall.

At smaller oscillation amplitudes, the regularity and repeatability seen in Fig. 4 vanish, indicating that for small-amplitude oscillations, stall is a somewhat random event. Even when the kinematic conditions are ripe for stall (in terms of instantaneous angle of attack, pitch rate, etc.), the airfoil may not stall unless an external event, such as a gust or vibration, occurs simultaneously. Otherwise the flow remains attached. This behavior is illustrated in Fig. 5. Figure 5a shows three time histories of the suction surface pressure at $x/c=0.012$ for $\alpha=8.5+2\sin\omega t$. The flow separates for only two of the six times when the angle of attack is greater than the static stall angle. The randomness of the stall process is even more striking for $\alpha=9.5+0.5\sin\omega t$, as shown in Fig. 5b. The flow state varies not only over short time scales (fractions of a period) but also over time scales of at least several oscillation cycles. The upper three time sequences in Fig. 5b correspond to a normally separated flow, which has occasional short periods of reattachment, while the bottom two time sequences exhibit the large negative suction peak pressure coefficients and relatively smooth behavior associated with attached flow. The data-taking procedure used in this experiment did not allow a large number of cycles to be taken continuously, so that no estimate of how rapidly the flow shifts between the stalled and unstalled states may be made. A similar effect was observed previously when an airfoil was held fixed near stall and the external flowfield oscillated in time.[11,12] In this case, the period of the alternation between the stalled and unstalled states was between 1 and 10 times the period of the imposed oscillation. In both experiments there is little observed correlation between imposed small-amplitude oscillations near the stall point and the instantaneous stalling and reattachment behavior.

Time histories of the pitching moment also show the variation between the stalled and unstalled states. For $\alpha=8+4\sin\omega t$ (Fig. 6a), the airfoil is usually unstalled, with short periods of stall, as shown by the large negative moments near the times of maximum angle of attack. For $\alpha=9.5+0.5\sin\omega t$ (Fig. 6b), there is no obvious correlation between the pitching moment and the instantaneous angle of attack. Nonetheless, as in Fig. 5b, the upper three sequences clearly represent predominantly separated flow with large random variations in the instantaneous moment, while the lower two sequences represent attached flow.

Hysteresis Loops

Hysteresis loops that cross-plot an aerodynamic coefficient against the instantaneous angle of attack are commonly used to illustrate periodic aerodynamic phenomena. Figure 7a shows an ensemble-averaged pitching moment loop for an airfoil oscillating in pitch between 1 and 17 deg at $k=0.1$. This figure is taken from previously unpublished data for the SC1095 airfoil. The loop may be divided into three subloops, two that trace counterclockwise curves as time increases and one that traces a central clockwise subloop. It has been shown previously[4] that clockwise pitching moment loops or subloops represent negative aerodynamic damping and would therefore cause oscillations of a free elastic airfoil to grow in amplitude, while counterclockwise loops would cause such oscillations to decay. For conditions such as in Fig. 7a, the area of the counterclockwise subloops is larger than that of the clockwise subloop, so that the overall oscillation would be damped.

For the smaller-amplitude oscillations studied in the current experiment, each individual loop tends to emphasize features found in particular regions of high-amplitude loops. Figure 7b shows an example of a moderate-amplitude pitch-

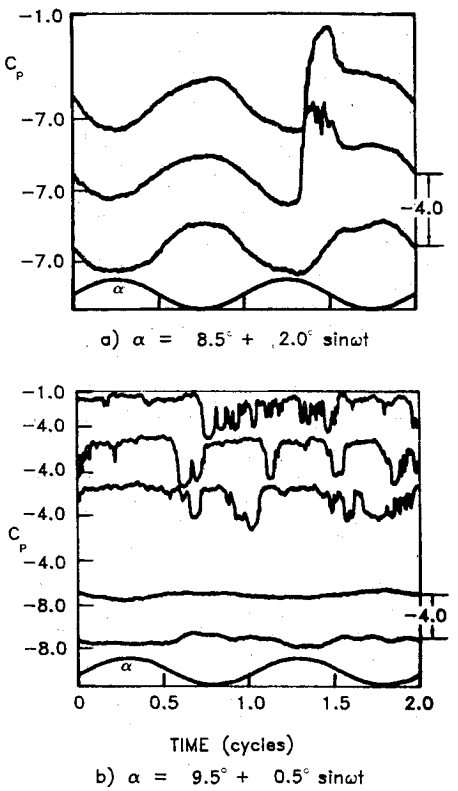

Fig. 5 Time histories of the suction surface pressure coefficient ($x/c=0.012$, $k=0.084$).

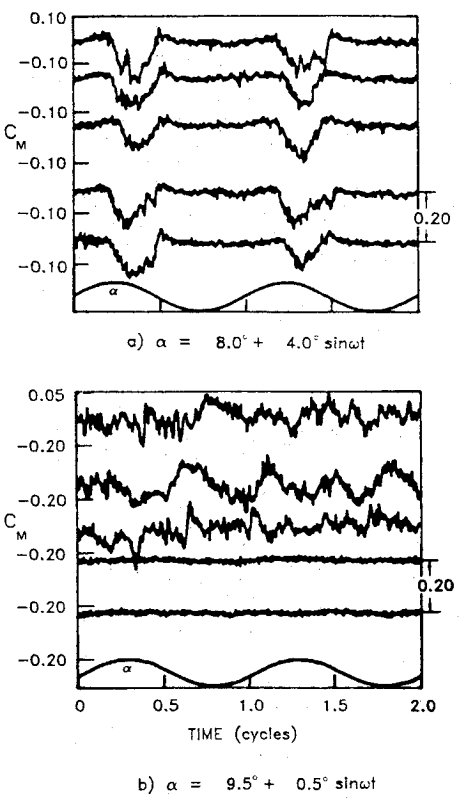

Fig. 6 Time histories of the pitching moment ($k=0.094$).

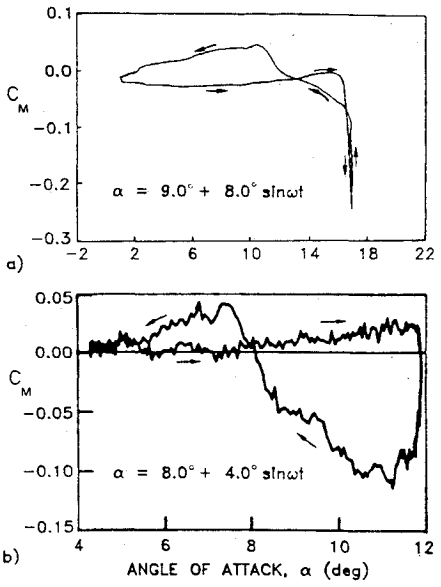

Fig. 7 Pitching moment loops at moderate amplitude ($k=0.094$).

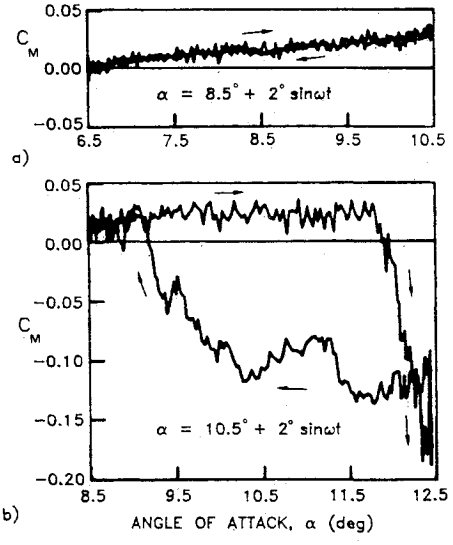

Fig. 8 Pitching moment loops at small amplitude ($k=0.094$).

ing moment loop, $\alpha=8+4\sin\omega t$ at $k=0.094$. There are two subloops, a counterclockwise ("stable") subloop for $\alpha<8$ deg, and a larger clockwise ("unstable") subloop at higher angles. Loops that cover different ranges of angle will emphasize different subloops, either stabilizing or destabilizing.

Loops for smaller-amplitude oscillations exhibit an even narrower range of features. If the airfoil remains unstalled over the entire oscillation cycle, the hysteresis is negligible, as shown in Fig. 8a for $\alpha=8.5+2.0\sin\omega t$. For oscillations near the stall angle, the pitching moment loop consists primarily of the central unstable loop, as shown in Fig. 8b for $\alpha=10.5+2\sin\omega t$. For oscillations at $\bar{\alpha}=0.5$ deg very close to stall, the appearance of the instantaneous loops differs depending on whether that particular cycle occurred when the airfoil was stalled or unstalled. This behavior was illustrated using time sequences in Figs. 5b and 6b. In addition to having a more negative mean level, a stalled loop has a greater hysteresis and a higher level of randomness. While this behavior seems to be typical of very small-amplitude loops, a more precise description would require acquiring many more ensembles of data (on the order of 100–500) to

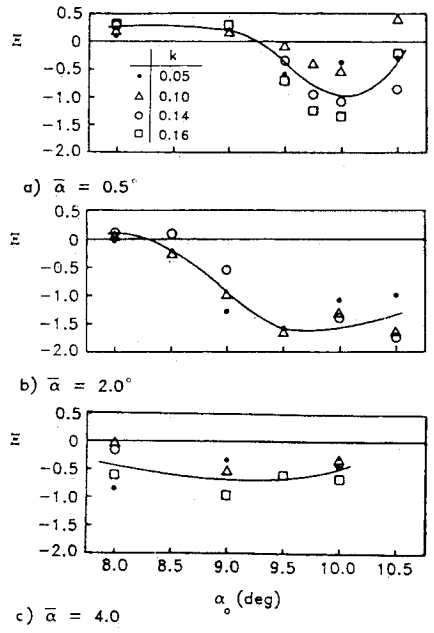

Fig. 9 Variation of pitch damping with mean angle.

determine what fractions of the time the flow is stalled or unstalled, and forming separate ensemble averages for the stalled, unstalled, and transitional conditions, a task well beyond the scope of this study.

Aerodynamic Damping

The transfer of energy between an oscillating airfoil and the surrounding airstream may be discussed more quantitatively in terms of a damping coefficient.[5] The net energy transfer for pitching motions is given by the work per cycle coefficient,

$$C_w = \oint C_M d\alpha \tag{1}$$

For a simple harmonic oscillation the damping coefficient is defined as

$$\Xi = -C_w/\pi\bar{\alpha}^2 \tag{2}$$

where positive damping implies an energy transfer from the airfoil to the airstream and negative damping implies that the airfoil receives energy from the air, causing the amplitude of the motion to increase with time. If the pitching moment coefficient is expressed as a Fourier series and substituted into Eq. (1), orthogonality leads to the following expression for the damping,

$$\Xi = -(C_{M_1}/\bar{\alpha})\sin\phi_1 \tag{3}$$

where C_{M_1} and ϕ_1 are the amplitude and phase of the moment coefficient at the fundamental frequency. The corresponding analytic expression for potential flow over thin airfoils[4] is $\Xi=\pi k/2$.

Figure 9 shows the experimentally measured damping plotted vs mean angle. As shown in Fig. 9a, at $\bar{\alpha}=0.5$ deg, there is only a narrow range of mean angles where the damping is negative, which would permit a small torsional disturbance to grow. Damping results at $\bar{\alpha}=2$ deg (Fig. 9b) show negative damping at mean angles >8 deg, about 1.75 deg below the static stall angle. Data were not taken at a high enough mean angle to determine the upper bound on the region of negative damping. At $\bar{\alpha}=4$ deg (Fig. 9c), the damping was always negative in the range of mean angles studied, between 8 and 10 deg. A rough approximation to

these results would be negative damping for $\alpha_{ss}-\bar{\alpha}<\alpha_0<\alpha_{ss}+\bar{\alpha}$ and positive damping elsewhere.

A Model for Aeroelastic Motion

The results of this experiment were used to model the process that might lead to stall flutter of an aircraft propeller during operation at high thrust and low forward velocity, when the blade angle of attack is near the stall angle. The simplest model for this situation is the single-degree-of-freedom torsional oscillation of a two-dimensional section. The aerodynamic pitch damping measured in this experiment can be used to determine whether an initial oscillation will grow, and if so, how rapidly.

The differential equation for this motion is[13]

$$I\ddot{\alpha}+K\alpha=M(\alpha) \tag{4}$$

The growth in amplitude of constant-frequency oscillations may be examined by forming an energy integral of this equation. This is accomplished by multiplying the equation by $d\alpha/dt$ and integrating over a single cycle of the motion n,

$$\left(\frac{I}{2}\left(\frac{d\alpha}{dt}\right)^2+\frac{K}{2}\alpha^2\right)\Bigg|_{\omega t=n\pi}^{\omega t=(n+1)\pi}=\oint_{\alpha_n}^{\alpha_{n+1}}M d\alpha \tag{5}$$

$$=-\pi\bar{\alpha}_n^2 qc^2\Xi_n$$

where the right-hand side is obtained from Eqs. (1) and (2). Since $\alpha=\alpha_0+\bar{\alpha}(t)\sin\omega t$, the left-hand side becomes

$$\frac{I\omega^2\bar{\alpha}^2}{2}\Bigg|_n^{n+1}=-\pi qc^2\bar{\alpha}^2{}_n\Xi_n \tag{6}$$

The change in amplitude over one cycle is therefore proportional to the product of a constant (composed of material and freestream properties) and the damping.

$$\bar{\alpha}^2\Big|_n^{n+1}=-\frac{2\pi qc^2}{I\omega^2}\Xi_n\bar{\alpha}_n^2=-C_{\Xi}\Xi_n\bar{\alpha}_n^2 \tag{7}$$

If, for simplicity, the blade section is approximated by a thin solid ellipse of constant material properties, the torsional moment of inertia and natural torsional frequency may be evaluated as

$$I=\frac{\pi\rho_m c^4\tau(2+\tau^2)}{64},\quad \omega_0=\frac{\pi}{2L}\sqrt{\frac{G}{\rho_m}}\frac{2\tau}{2+\tau^2} \tag{8}$$

Therefore, the constant in Eq. (7) becomes

$$C_{\Xi}=\frac{128}{\pi^2}\frac{(2+\tau^2)}{\tau^3}AR^2\frac{q}{G} \tag{9}$$

Equation (7) may now be solved for any given set of material and aerodynamic properties to determine how an initial oscillation will develop. The use of the energy integral technique allows a simple equation to be obtained, but only provides information on the growth of the envelope amplitude ($\bar{\alpha}$) and does not account for nonlinear effects that would alter the frequency or harmonic character of the oscillation.

A series of calculations were made to study the growth of an initial 0.25-deg-amplitude oscillation. The damping (Fig. 10) was assumed to be a combination of the amplitude-dependent aerodynamic damping and a constant material damping coefficient of +0.13 (arbitrarily chosen to provide a small shift from zero damping). The aerodynamic damping was based on the maximum negative damping measured for each value of $\bar{\alpha}$ in the current test (Fig. 9) and, for higher

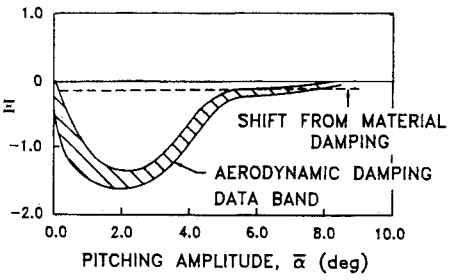

Fig. 10 Pitch damping results for use in aeroelastic calculation.

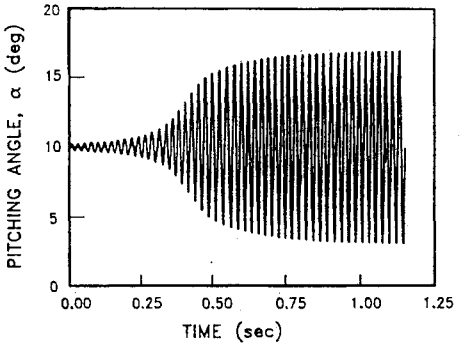

Fig. 11 Calculated pitching time history ($C_{\Xi}=0.43$).

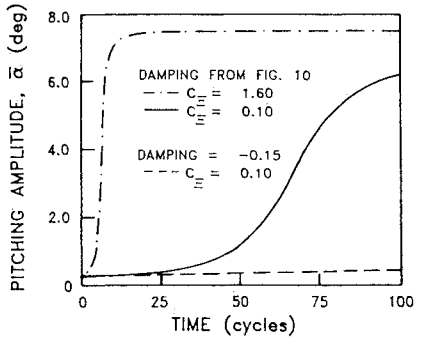

Fig. 12 Calculated growth of pitching oscillation amplitude.

amplitudes, the results of Ref. 5. The combination of material and aerodynamic damping results in zero net damping at $\bar{\alpha}=7.5$ deg, which therefore becomes the limiting amplitude for this example.

Figure 11 shows the calculated time history of the angle of attack for a solid aluminum elliptical airfoil that is 5% thick, has an aspect ratio of 6, and is operating at a Mach number of 0.14. Note that the methods used in this example are based solely on two-dimensional low-airspeed damping data, so that the Mach number serves only to establish the dynamic pressure (at sea-level conditions), and the aspect ratio serves only to determine the natural torsional frequency (42 Hz in this case). The model problem makes no attempt to include the effects of compressibility or three-dimensionality. With these limitations, and assuming that the oscillation is at the natural frequency, this model predicts that $\bar{\alpha}$ will grow from the initial value of 0.25 deg and approach the limit-cycle amplitude of 7.5 deg in about 50 cycles, or 1 s.

The fundamental character of the amplitude growth profile for this model is always the same. Depending on the value of C_{Ξ} (and therefore on Mach number, aspect ratio, thickness ratio, and material density), the number of cycles required for growth from 0.25 to 7.5 deg will vary. For the

case shown in Fig. 11, $C_{\Xi} = 0.40$. The growth of the oscillation amplitude is shown in Fig. 12 for $C_{\Xi} = 0.10$ (solid line) and for $C_{\Xi} = 1.60$ (dash-dot line).

The disturbance grows much more slowly if the maximum negative aerodynamic damping, instead of reaching the value of -1.5, is limited to a value of -0.15 (the value determined from the higher-amplitude oscillations of Ref. 5). As shown by the dashed line in Fig. 12, an initial 0.25-deg-amplitude disturbance has grown to less than 0.30 deg after 100 cycles. For this type of damping profile, flutter would require either an unreasonably long time to develop or a much larger initial disturbance.

Summary and Conclusions

An initial experiment has been performed to study the aerodynamics of small-amplitude airfoil oscillations near stall. The purpose of the experiment was to obtain insight into the mechanisms involved in the development of stall flutter from incipience.

Time histories of the pressure, normal force, and pitching moment response indicated that regions of stalled and unstalled flow are clearly defined by changes in both the mean level and the intensity of the small time-scale (turbulent) variations. The transition between these regions (separation and reattachment) was sudden. At higher oscillation amplitudes ($\bar{\alpha} \geq 4$ deg), separation and reattachment were well correlated with the instantaneous angle of attack, while at lower amplitudes the stall process was much more random and was probably triggered by external events such as a gust or vibration.

Hysteresis loops of normal force and pitching moment vs angle of attack are highly dependent on mean angle and oscillation amplitude. At small amplitude there is little hysteresis either below or above stall (i.e., for $\bar{\alpha} + \alpha_0 < \alpha_{ss}$ or $\bar{\alpha} - \alpha_0 > \alpha_{ss}$), but near stall the hysteresis was large, and in particular, the pitching moment loops were dominated by a central clockwise subloop. Such behavior implies that energy would be transferred from the airstream to an unrestrained airfoil, leading to growth in the amplitude of oscillations. This behavior was confirmed by calculation of the aerodynamic pitch damping, which reached large negative values ($-1 < \Xi < -2$) for oscillation amplitudes near 2 deg and mean angles near the stall angle.

The measured aerodynamic damping was used to compute the growth in amplitude of a single-degree-of-freedom torsional oscillation of a two-dimensional airfoil. The growth rate was found in this simple model problem to be a product of the net damping times a constant that depended on material and freestream properties. Calculations made using representative values of this constant show that, when the mean angle is close to the stall angle, an initial small-amplitude oscillation will grow rapidly, taking between 15 and 100 cycles to develop into a high-amplitude limit-cycle oscillation. This rapid growth is not present when the maximum negative damping is limited to the values observed at higher oscillation amplitudes ($\Xi = -0.15$).

While the present experiment has provided considerable information on the aerodynamics of small-amplitude oscillations near stall and has established a mechanism that may describe the onset of stall flutter, more definitive data will be required to produce a quantitative description of the phenomena, to determine the parameters that influence the airfoil stability characteristics, and to influence the design process directly. To model conditions on modern propeller blades more accurately, data should be obtained using thinner airfoil sections and at increased Mach number, Reynolds number, and reduced frequency.

Acknowledgments

This work was supported by United Technologies Research Center corporate funding and was assisted by additional funds from the Hamilton Standard Division of United Technologies Corporation.

References

[1]Baker, J.E., "The Effects of Various Parameters, Including Mach Number, on Propeller-Blade Flutter with Emphasis on Stall Flutter," NACA RML50L12b, 1950; reissued as NACA TN 3357, Jan. 1955.

[2]Fanti, R., Carta, F.O., and Pitt, W.R., "Stall-Flutter Characteristics of Several 16-Series Cantilevered Airfoil Models," United Aircraft Corporation Research Department Rept. R-23624-2, East Hartford, CT, May 1954.

[3]Lemnios, A.Z., "Aerodynamic Damping Tests of Propeller Blade Airfoil Sections," United Aircraft Corporation Research Department Rept. R-0997-1, East Hartford, CT, Oct. 1957.

[4]Carta, F.O. and Niebanck, C.F., "Prediction of Rotor Instability at High Forward Speeds. Volume III. Stall Flutter." USAAVLABS Tech. Rept. 68-18C, U.S. Army Aviation Material Laboratories, Ft. Eustis, VA, Feb. 1969.

[5]Carta, F.O., "A Comparison of the Pitching and Plunging Response of an Oscillating Airfoil," NASA CR-3172, Oct. 1979.

[6]St. Hilaire, A.O., Carta, F.O., Fink, M.R., and Jepson, W.D., "The Influence of Sweep on the Aerodynamic Loading of an Oscillating NACA 0012 Airfoil. Vol. I, Technical Report," NASA CR-3092, May 1979.

[7]McCroskey, W.J., McAlister, K.W., Carr, L.W., and Pucci, S.L., "An Experimental Study of Dynamic Stall on Advanced Airfoil Sections. Volume I. Summary of the Experiment," NASA TM 84245, USAAVRADCOM TR-82-A-8, U. S. Army Air Mobility Research and Development Laboratory, Ft. Eustis, VA, July 1982.

[8]St. Hilaire, A.O. and Carta, F.O., "Analysis of Unswept and Swept Wing Chordwise Pressure Data From an Oscillating NASA 0012 Airfoil Experiment. Volume I. Technical Report," NASA CR-3567, March 1983.

[9]McCroskey, W.J., "Some Current Research in Unsteady Fluid Dynamics—The 1976 Freeman Scholar Lecture," *Journal of Fluids Engineering,* Vol. 99, March 1977, pp. 8-39.

[10]Carta, F.O., "An Experimental Investigation of Gapwise Periodicity and Unsteady Aerodynamic Response in an Oscillating Cascade. I—Experimental and Theoretical Results," NASA CR-3513, June 1982.

[11]Vaczy, C.M., "Unsteady Separated Flow Fields around a NACA 0012 Airfoil," S.M. Thesis, Department of Aeronautics and Astronautics, M.I.T., Cambridge, MA, May 1984.

[12]Covert, E.E., Lorber, P.F., and Vaczy, C.M., "Flow Separation Induced by Periodic Aerodynamic Interference," *Proceedings of the AFOSR/FJSRL/U.* Colorado Workshop on Unsteady Separated Flows, Aug. 10-11, 1983.

[13]Bisplinghoff, R.L., Ashley, H., and Halfman, R.L., *Aeroelasticity,* Addison-Wesley, Reading, MA, 1955.